

DOI 10.24425/aee.2023.146052

Analysis and effect of static eccentricity fault on performance indicators of a synchronous reluctance motor

EMMANUEL IDOKO¹, GIDEON DAVID UM OH², PAULINE IJEOMA OBE³, BENJAMIN OKWUDILI MAMA⁴, EMEKA SIMON OBE⁵

¹Department of Electrical and Electronics Engineering, Federal University of Agriculture
970101 Makurdi, Benue State, Nigeria

²Department of Electrical Engineering, Maritime Academy
523101 Oron, Akwa Ibom State, Nigeria

³Department of Industrial Technical Education, University of Nigeria
410001 Nsukka, Enugu State, Nigeria

⁴Department of Civil Engineering, University of Nigeria
410001 Nsukka, Enugu State, Nigeria

⁵Department of Electrical, Electronic and Telecommunications Engineering
Botswana International University of Science and Technology
Plot 10071 Boseja, Palapye, Botswana

e-mail: emmanuel.idoko@uam.edu.ng, umohgideon@gmail.com,
pauline.obe/benjamin.mama@unn.edu.ng, obe@biust.ac.bw

(Received: 15.02.2023, revised: 26.06.2023)

Abstract: Fault diagnosis and condition monitoring of synchronous machines running under load is a key determinant of their lifespan and performance. Faults such as broken rotor bars, bent shafts and bearing issues lead to eccentricity faults. These faults if not monitored may lead to repair, replacement and unforeseen loss of income. Researchers who attempted to investigate this kind of machine stopped at characterizing and deduced ways, types and effects of rotor eccentricity fault on the machine inductances using the winding function method. A modified closed-form analytical model of an eccentric synchronous reluctance motor (SynRM) is developed here taking into cognizance the machine dimensions and winding distribution for the cases of a healthy and unhealthy SynRM. This paper reports the study the SynRM under static rotor eccentricity using the developed analytical model and firming up the model with finite element method (FEM) solutions. These methods are beneficial as they investigated and presented the influence of the degrees of static eccentricity on the machine performance indicators such as speed, torque and the stator



© 2023. The Author(s). This is an open-access article distributed under the terms of the Creative Commons Attribution-NonCommercial-NoDerivatives License (CC BY-NC-ND 4.0, <https://creativecommons.org/licenses/by-nc-nd/4.0/>), which permits use, distribution, and reproduction in any medium, provided that the Article is properly cited, the use is non-commercial, and no modifications or adaptations are made.

current and assess the extent to which the machine performance will deteriorate when running with and without load. The results show that static eccentricity significantly affects the machine’s performance as the degree of eccentricity increases.

Key words: degree of eccentricity, faults, finite element method, inductances, static eccentricity, synchronous reluctance motor, winding function

1. Introduction

Synchronous machines are undoubtedly very useful in many facets of industrial applications. Their performance is more sensitive in special applications. The synchronous reluctance motor (SynRM) as a member of this family is popular now because of its unique features. SynRM is robust, it requires no rotor windings and a permanent magnet for excitation, which makes it cheaper than permanent magnet motors and is more efficient due to the absence of rotor copper loss; it has high fault tolerance capability. Even with these qualities, stator winding faults, broken rotor bar faults, bearing faults, rotor eccentricity faults, etc. are major faults that affect SynRM general performance [1]. The rotor eccentricity fault occurs as a result of bearing offset or stator deformation during the manufacturing and assembly stage which causes the air gap to be unevenly distributed. The fault constitutes 70–80% of mechanical faults in the industry, therefore, it is important to precisely monitor and characterize this kind of fault to avoid its escalation [2].

Eccentricity is majorly made up of static eccentricity (STE) and dynamic eccentricity (DYE). The two co-exist to form the combined eccentricity (CME). Figure 1 shows how the three types of eccentricities operate.

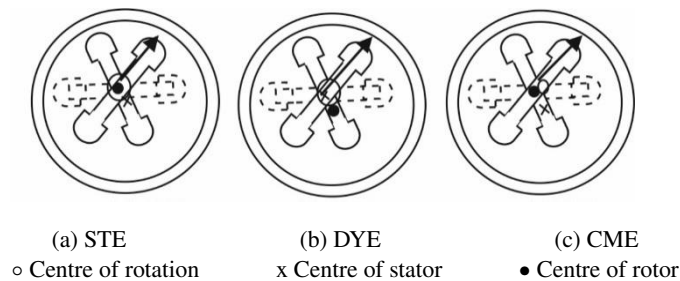


Fig. 1. (a) STE; (b) DYE; (c) CME

Several techniques have been adopted by researchers in analysing SynRMs [2–6]. To keep the machine’s healthy operation in check, constant monitoring of some performance indicators’ characteristics needs to be examined frequently to assess the motor’s general performance. Some research work has been established in the areas of modelling, analysing, and detecting the eccentricity fault in induction motors [7–9] and permanent magnet motors [10–12]. Popular among the techniques applied to calculate the machine inductances are the winding function method (WFM) and the modified winding function method (MWFM). The WFM is mostly adopted for a healthy machines whose air gap is symmetrical or uniform [3, 15]. The MWFM is largely adopted for faulty machines since it accounts for air gap eccentricity [5, 17, 18]. The work of [29] revealed

that Modified Winding Function Theory (MWFTh) is generally accepted in analyzing rotating electrical machines which have a very small air gap. The authors further stated that two different approaches showed that the high-rated MWFTh formula is not applicable in analyzing machines with large air gaps. Majority of the researchers who investigated faulty machines patronized this method. The calculations of inductances of salient-pole synchronous motor operating under eccentricity using MWFTh were done by [17, 20] and [21]. Again [21] developed an analytical model that can compute the machine inductances under any kind of eccentricity. The method was based on MWFA which took into account the variable air gap functions, the flux fringing effects, slots effects and the three-dimensional distribution of machine windings. Instead of the application of a modified winding function in calculating the machine inductances, a closed form of the Fourier series expansion equation was developed by [22] which took into account all the space harmonics to calculate the inductances. These results were verified with the FEM which showed good agreement. Hwang *et al.* [23] investigated and compared the effect of rotor eccentricity on magnetic flux density, average and cogging torque using a transient finite element model for two three-phase, 6-pole, 36-slot IPM and surface-mounted synchronous motors. The results were compared with those obtained from a symmetric rotor machine but [24] developed a fundamental model that is based on sensor-less control of PM synchronous machine (PMSM) under rotor eccentricity to investigate the effects of rotor eccentricity on inductances, flux linkage and back E.M.F characteristics. The results showed that these indexes were grossly affected. Takahata and Wakui [25] employed the finite element method (FEM) to investigate the effect of rotor eccentricity on interior permanent magnet motor (IPMSM), it was concluded that IPMSM with rotor eccentricity caused an increase in radial electromotive force and higher vibration acceleration when compared with the healthy machine. The FEM is mostly used for modelling or validating other results. Iamamura *et al.* [26] used the 2D and 3D-FEMs to detect the presence of static and dynamic eccentricity on a synchronous generator and concluded that the methods could identify the type of eccentricity affecting the machine while [27] investigated the torque profile of a dynamic eccentric switched reluctance motor using 2D-FEM at different value of currents. It was discovered that the torque increased as the rated current values increased. The report in [11] used the FEM to validate all the results obtained from the analytical model at each stage of calculations for concentrated windings PM synchronous machines with rotor eccentricity, but [28] investigated how the presence of dynamic air gap eccentricity affected the inductances and induced harmonics on the stator current of a salient pole synchronous machine with a faulty rotor. The machine winding inductances were calculated using a modified winding function approach. In Dorgan *et al.* [33] the effect of static eccentricity was investigated in LSPMSM using the finite element method under load condition. The results show that, as the values of eccentricity increased, the stator current also increased. Tootoonchian *et al.* [29] studied the effect of static eccentricity using an analytical model and modern control rudiments by modelling the eccentricity resolver which was based on a d - q synchronous coordinate system by varying the values of d -axis and q -axis inductances (L_d and L_q). The results showed that the accuracy of the resolver was affected by the presence of eccentricity. Bessou *et al.* [30] investigated the effect of static eccentricity fault using the motor vibration signature analysis for detecting the fault and the motor current signature analysis for establishing the type. The stator current was analyzed using a fast Fourier transform and discrete wavelet transform. The author's results showed that static eccentricity causes acoustic noises and leads to flux density vibrations which were seen in the

stator current spectrums. Aggarwal and Strangas [32] further applied four different methods to investigate static eccentricity in IPMSM. El M. *et al.* [34] investigated mixed eccentricity fault based on the neutral voltage between the main supply and the stator. The authors' results show that the line neutral voltage spectrum is subtle to air gap eccentricity compared to the stator current spectrum. In the case of Wronski *et al.* [31], the authors applied the starting phase current to investigate static and dynamic eccentricities using the discrete wavelet transform (DWT) and transient motor current signature analysis (TMCSA) methods. The results from the application percentage energy of DWT showed that dynamic eccentricity causes a rise in percentage energy while static eccentricity leads to a decrease in percentage energy.

It is obvious from the findings that detailed work on the effect of static eccentricity on synchronous reluctance motor performance has not been explored. But enormous publications on eccentricity fault detection and modelling of induction machines have been recorded [37]. The majority of the researchers who attempted to investigate the synchronous reluctance machine stopped at finding the effect of eccentricity fault on the inductances using the WEM while others employed the stator current spectrum as the performance indicator to characterized and find the types and effects of rotor eccentricity fault on the machine.

The purpose of this paper is to investigate the performance indicators of SynRM in terms of speed, torque and stator current under static rotor eccentricity using a developed analytical model and to validate the results with finite element method solutions to assess to what degree are the indicators affected.

The procedure adopted here is to characterize the machine geometry completely and introduce an analytical measure of eccentricity in a form in which it becomes a variable in the airgap model. This is included in the airgap geometrical information as a variable displacement from the rotor set-point center. The degree of this displacement variable determines the level of eccentricity. Inductances are calculated by using the modified winding function (MWF) approach. Analytical model was then developed in phase variables to include this actual rotor airgap information and then the machine performance is studied by dynamic simulation in Simulink®. The effect of these changes is then observed in the machine operational indices like inductances, current, torque and speed departures from normal.

For this purpose, the article has been organized into the following Sections. The SynRM with uniform and distorted air gaps described in Section 2, shall be modelled from a developed algorithm to judge their winding symmetries using the motor. Section 3 will present the model inductances expressions and plots calculated to exhibit the presence of rotor airgap variations on the inductances. Section 4 presents the model equations developed in phase variable form to assess the machine performance. Section 5 presents the digital simulation results for the performance indices of the developed phase variable model and finite element method while the discussion of the results is in Section 6. Finally, the conclusion is given in Section 7.

2. Analysis of SynRM with non-uniform airgap

The analysis of this machine begins with the modelling of the air gap because of the misalignment of the rotating members (rotor, shaft and rotor bars) of the machine from the stator centre. The results of the inverse air gap model are mostly needed for evaluating the machine inductances.

These values are employed for calculating the healthy and faulty machine inductances considering the rotating members' new positions.

The machine under study in Fig. 2 is a 380 V, 5.5 kW three-phase, 36-slots, 4-pole salient pole rotor SynRM with uniform (the point where all the axes coincide) and non-uniform air gap distributions shown arbitrarily for the sake of analysis. Figure 2 was used for the analytical model. The shift of the rotor members from their mutual centres; created an unequal distribution of air gaps. These shifts are for 0.04, 0.08, . . . , 0.32 mm which represent 10%, 20%, . . . , 80% of the air gap length of 0.4 mm of the motor from their mutual centre. In this context, the modelling and analysis shall cover the percentage values of different degrees of eccentricities for the machine with uniform and distorted air gaps.

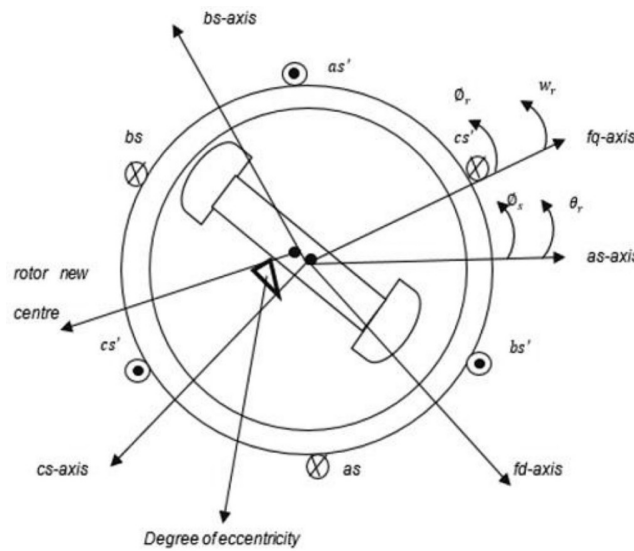


Fig. 2. SynRM with 4-pole salient rotor

2.1. Modelling of the inverse air gap

It has been mentioned that the rotor members shall be shifted eight times to create an uneven distribution of the air gaps for a specified degree of eccentricity faults. The effective air gap model equations for the healthy and static eccentric machine can be deduced respectively as:

$$g(\theta_s, \theta_r) = \frac{1}{\Delta_1 - \Delta_2 \cos 2(\theta_s - \theta_r)}, \tag{1}$$

$$g(\theta_s, \theta_r) = \frac{(1 - \partial_s \cos(\theta_s))}{\Delta_1 - \Delta_2 \cos 2(\theta_s - \theta_r)}. \tag{2}$$

The inverse air gap model equations were gotten by modifying (1) and (2) as shown.

$$g^{-1}(\theta_s, \theta_r) = \Delta_1 - \Delta_2 \cos 2(\theta_s - \theta_r), \tag{3}$$

$$g^{-1}(\theta_s, \theta_r) = \frac{\Delta_1 - \Delta_2 \cos 2(\theta_s - \theta_r)}{(1 - \partial_s \cos(\theta_s))}, \tag{4}$$

where $\Delta_1 = \frac{1}{2} \left(\frac{1}{g_0} + \frac{1}{g_1} \right)$ and $\Delta_2 = \frac{2}{\pi} \left(\frac{1}{g_0} - \frac{1}{g_1} \right) \sin \pi \beta$ from which g_0 is the main air gap length at pole face, g_1 inter-polar slot space and β is the ratio of pole arc to pole pitch respectively, θ_s is the stator circumferential angle, θ_r is the rotor angle position and ∂_s is the degree of static eccentricity.

These models in (3) and (4) of the air gap were plotted in a MATLAB environment using the machine dimensions of the healthy SynRM in Table 1. Figure 3 shows the values of the result of the air gap functions model operating at the specified degrees of eccentricity faults.

Equation (4) is approximated as reported by [35] as

$$g^{-1}(\theta_s, \theta_r) = \frac{1}{g_0 \sqrt{1 - \partial_s^2}} + \frac{2}{g_0 \sqrt{1 - \partial_s^2}} \left(\frac{1 - \sqrt{1 - \partial_s^2}}{\partial_s} \right) \cos(\theta_s). \quad (5)$$

Table 1. Synchronous reluctance motor parameters [20]

Parameter name	Symbol	Value	Unit
Stator outer/inner radius	R_{so}	105	mm
Stator inner radius	R_{si}	67.99	mm
Rotor radius	r	67.59	mm
Effective stack length	l	106.22	mm
Permeability of free space	μ_0	$4\pi \times 10^{-7}$	H/m
Air gap length at the pole	g_0	0.40	mm
Interpolar slot depth	g_1	6.50	mm
Stator slot depth	τ_d	18.00	mm
Pole arc to pole pitch ratio	β	2/3	–
Number of pole pairs	p	2	–
Number of stator slots	–	36	–
Frequency	f	50	Hz
Number of rotor cage pars per pole	–	6	–
Stator resistance	R_s	0.62	Ω
Stator leakage inductance	L_{ls}	8.30	mH
Rotor q -axis leakage inductance	L_{lqr}	6.20	mH
Rotor d -axis leakage inductance	L_{ldr}	5.50	mH
Rotor q -axis resistance	R_{qr}	0.12	Ω
Rotor d -axis resistance	R_{dr}	0.12	Ω
Moment of inertia	J	0.089	kgm ²
Number of turns	N	32	–
Stator slot pitch	τ	14.00	mm

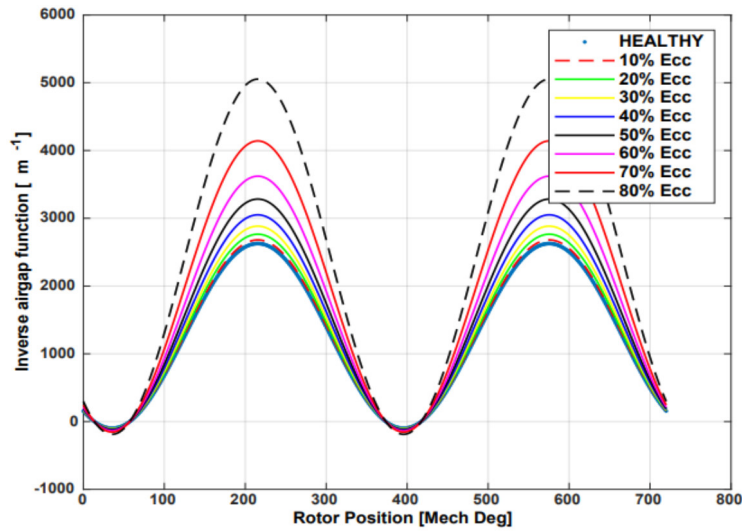


Fig. 3. Inverse air gap functions for healthy and 10% to 80% eccentric SynRM

2.2. Winding function model

According to [3], the inductance between any two windings on a rotating ac machine is given by:

$$L_{ij}(\theta_r) = \mu_o r l \int_0^{2\pi} \frac{1}{g(\theta_s, \theta_r)} N_i(\theta_s) N_j(\theta_s) d\theta_s, \quad (6)$$

where μ_o is the permeability of free space, r is the radius of the rotor, l is the stack length of the machine, $N_i(\theta_s)$ and $N_j(\theta_s)$ are the winding functions for windings i and j respectively, g is the air gap function. The fundamental components of N_i and N_j of any of the stator windings can be gotten from:

$$N_i(\theta_s) = \frac{N_{HH} k_{wn}}{p_r} \cos\left(\theta_s - k \frac{2\pi}{p_r m}\right). \quad (7)$$

$k = 0, 2, 4, \dots$ for phases A, B and C, respectively, p_r represents the pole pairs, $k_{wn} \approx 1$, m is the number of phases and N_{HH} is the healthy winding function.

According to [36], the fundamental components of the cage rotor winding function of the machine can be obtained by aligning the rotor pole axis with any of the stator phase axes in direct and quadrature axes as:

$$N_q(\theta_s, \theta_r) = N_{qr} \cos(\theta_r - \theta_s), \quad (8)$$

$$N_d(\theta_s, \theta_r) = N_{dr} \sin(\theta_r - \theta_s), \quad (9)$$

where:

$$N_{qr}(\theta_s, \theta_r) = \frac{8}{\pi} \left[n_m - \cos\left(\gamma \frac{N_b - 1}{2}\right) n_q \right] \sin^2 \frac{\gamma}{2} \cos \beta,$$

$$N_{dr}(\theta_s, \theta_r) = \frac{2}{\pi} \left[n_m + 2 \sin^2 \frac{\gamma}{2} - \cos(n_p \gamma) n_q \right] \sin \beta,$$

$$n_m = 0.5N_b - 1, \quad n_p = 0.5N_b + 1; \quad n_q = \frac{\sin(n_m\gamma)}{\sin \gamma},$$

where: $\beta = (\theta_r - \theta_s)$; N_b is the number of rotor bars per pole, γ is the rotor slot span, $N_q(\theta_s, \theta_r)$ is the q -axis rotor winding function, $N_d(\theta_s, \theta_r)$ is the d -axis rotor winding function.

2.3. Modified winding function method

The modified winding function method (MWF) is widely accepted for computing faulty machine inductances [17, 18, 38]. The expression of the MWF is shown as

$$M(\theta_s, \theta_r) = n(\theta_s, \theta_r) - \langle M(\theta_s, \theta_r) \rangle, \quad (10)$$

where: $M(\theta_s, \theta_r)$ is the modified winding function, $n(\theta_s, \theta_r)$ is the turn function and $\langle M(\theta_s, \theta_r) \rangle$ is the average value of the MWF.

$$\langle M(\theta_s, \theta_r) \rangle = \frac{1}{2\pi \langle g^{-1}(\theta_s, \theta_r) \rangle} \int_0^{2\pi} n(\theta_s, \theta_r) g^{-1}(\theta_s, \theta_r), \quad (11)$$

$$\langle g^{-1}(\theta_s, \theta_r) \rangle = \frac{1}{2\pi} \int_0^{2\pi} g^{-1}(\theta_s, \theta_r) d\theta_s, \quad (12)$$

$$n_i(\theta_s) = N_i(\theta_s) - \frac{N_{HH}}{2}, \quad (13)$$

$\langle g^{-1}(\theta_s, \theta_r) \rangle$ is the average value of the inverse air gap function.

The value of (10) is obtainable by substituting the values of the solution of (11) to (13). These calculations were done in the 2018b MATLAB® environment. Obtaining these values helped in solving for the self and mutual inductance expression for the eccentric SynRM.

Similarly, the inductance between any two phases of the windings under eccentricity conditions can be evaluated using

$$L_{ij}(\theta_r) = k \left[\int_0^{2\pi} n_i(\theta_s, \theta_r) n_j(\theta_s, \theta_r) g^{-1}(\theta_s, \theta_r) d\theta_s - av \right], \quad (14)$$

where $av = 2\pi \langle M_{iS}(\theta_s, \theta_r) \rangle \langle M_{jS}(\theta_s, \theta_r) \rangle \langle g^{-1}(\theta_s, \theta_r) \rangle$ and $k = \mu_o r l$.

SL_{ijS} represents the inductances between phase i and j of the eccentric machine.

3. Inductance computations

This section presents detailed inductance computations of the healthy and eccentric SynRM. The term self and mutual inductances encompasses that of the stator and rotor. The self and mutual inductances L_{asas} , L_{asbs} , \dots , L_{drdr} for the healthy SynRM were obtained from equation (6). Similarly, the self and mutual inductances L_{asas} , L_{asbs} , \dots , L_{drdr} for the faulty SynRM

inductances were found using (14). The inductance expression of (6) was solved by substituting the values of the winding functions in (7) to (9) while (14) was solved in a similar vein as mentioned in Section 2.3. The values of the machine geometries were taken from Table 1. The inductance plots for the healthy and eccentric SynRM are combined for the sake of brevity and comparison as shown in Figs. 4 to 8.

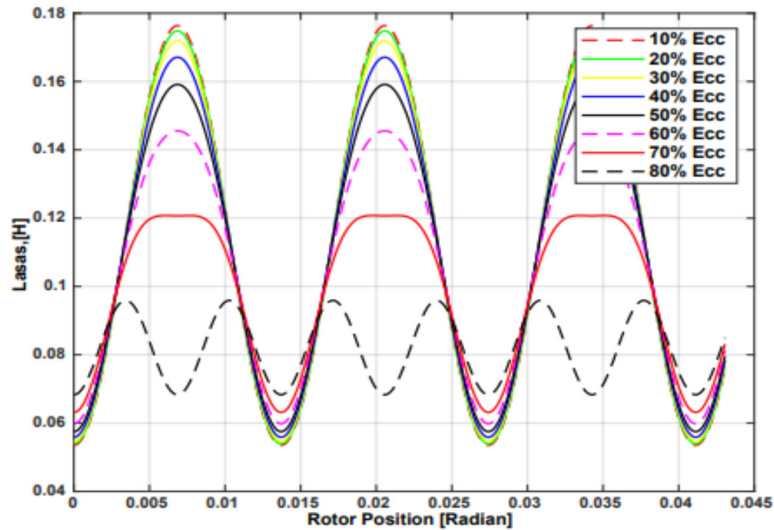


Fig. 4. Phase A stator self-inductances for healthy and 10% to 80% static eccentricity fault

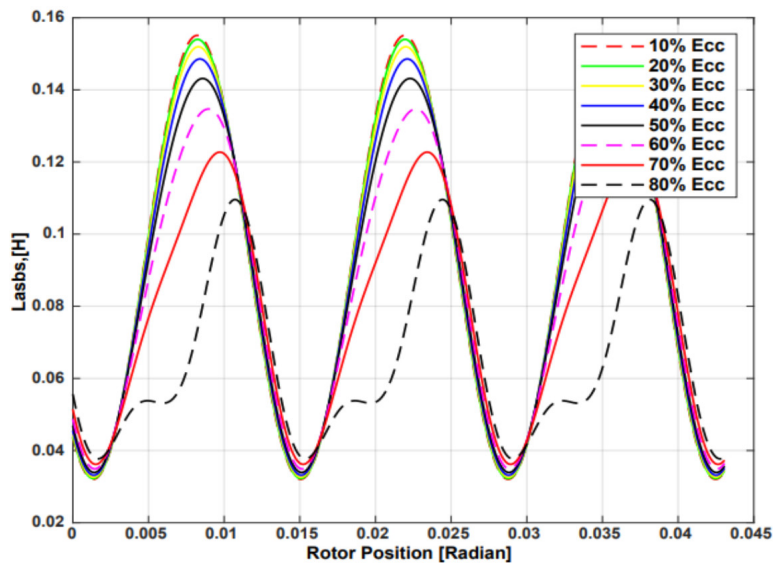


Fig. 5. Phase A and B stator mutual inductances for healthy and 10% to 80% static eccentricity fault

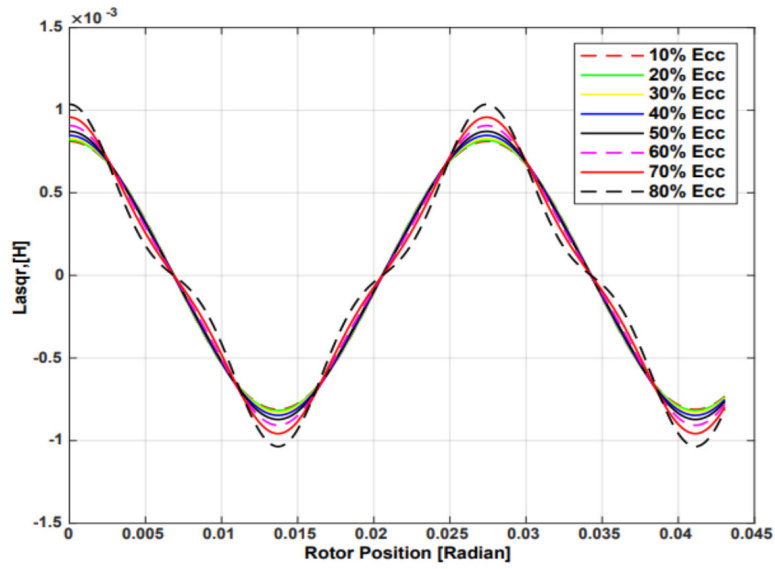


Fig. 6. Phase A and q -axis stator-rotor mutual inductances for healthy and 10% to 80% static eccentricity fault

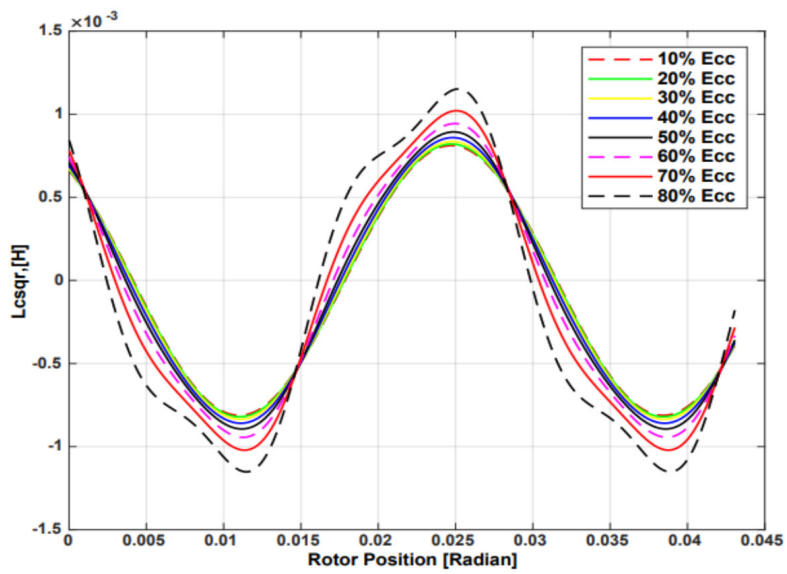


Fig. 7. Phase C and Q stator-rotor mutual inductances for healthy and 10% to 80% static eccentricity fault

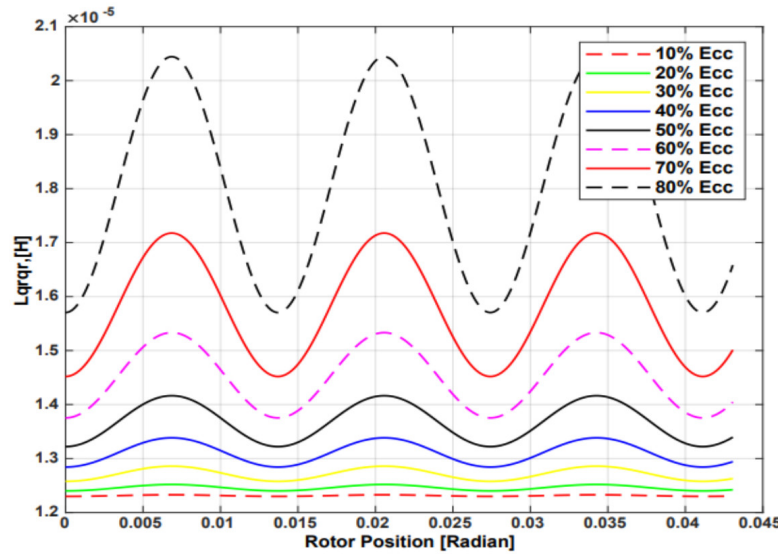


Fig. 8. q -axis rotor self-inductances for 10% to 80% static eccentricity fault

4. Dynamic model expressions for the healthy and static eccentric SynRM

4.1. Phase variable model

The motor performance is predicted by solving its set of differential equations for stator current, electromagnetic torque and speed using the phase variable model. The inductances obtained in the previous section were set up in matrix form considering the stator phases a , b and c and the rotor d and q equivalent windings for the healthy and static eccentric SynRM. Using common electrical machine symbols and parlances (I for currents, V for voltages and R for resistances), the machine voltage equation is:

$$V = IR + \frac{d}{dt} (L(\theta_r)I) \tag{15}$$

or simply

$$\frac{dI}{dt} = \frac{1}{L(\theta_r)} \left(V - I \left(R + \omega_r \frac{dL(\theta_r)}{d\theta_r} \right) \right), \tag{16}$$

where

$$V = [V_a \ V_b \ V_c \ V_q \ V_d]^T, \quad I = [I_a \ I_b \ I_c \ I_q \ I_d]^T,$$

$$R = \text{diag} [R_a \ R_b \ R_c \ R_q \ R_d]$$

and $L(\theta_r)$ is the inductance matrix given as:

$$L(\theta_r) = \begin{bmatrix} L_{aa} & L_{ab} & L_{ac} & L_{aq} & L_{ad} \\ L_{ba} & L_{bb} & L_{bc} & L_{bq} & L_{bd} \\ L_{ca} & L_{cb} & L_{cc} & L_{cq} & L_{cd} \\ L_{qa} & L_{qb} & L_{qc} & L_{qq} & L_{qd} \\ L_{da} & L_{db} & L_{dc} & L_{dq} & L_{dd} \end{bmatrix}.$$

The developed electromagnetic torque is:

$$T_e = \frac{1}{2} I_S^T \times \frac{dL_S}{d\theta_r} \times I_S + I_S^T \times \frac{dL_{SR}}{d\theta_r} \times I_R, \quad (17)$$

where: $I_S = [i_a \ i_b \ i_c]^T$ is the stator currents, $I_R = [i_q \ i_d]^T$ is the rotor currents, L_{SS} is the first (3×3) partition matrix of $L(\theta_r)$ representing the stator inductances and L_{SR} is the (2×3) partition matrix of stator-to-rotor mutual inductances given as:

$$L_{SS} = \begin{bmatrix} L_{aa} & L_{ab} & L_{ac} \\ L_{ba} & L_{bb} & L_{bc} \\ L_{ca} & L_{cb} & L_{cc} \end{bmatrix} \quad \text{and} \quad L_{SR} = \begin{bmatrix} L_{aq} & L_{ad} \\ L_{bq} & L_{bd} \\ L_{cq} & L_{cd} \end{bmatrix}.$$

Neglecting the effect of friction, rotor speed and torque are related as:

$$\frac{d\omega_r}{dt} = J (2/p) (T_e - T_L), \quad (18)$$

where T_L is the load torque, p is the number of pole pairs and J is the total inertia of the rotating mass. These equations can be solved for the healthy and the eccentric machine by careful substitution of the calculated inductances for each specific case from Section 3.

4.2. Finite element model

The ANSYS RMxpTM is a tool used for designing the motor based on the machine dimensions. Table 1 was employed in this case, the materials used for the stator, shaft and rotor are M19_24 steel type, the rotor bars used Aluminium_75C while the stator coils used copper_75C. After the design, the RMxpTM was exported to Maxwell-2D to allow the analysis of the machine performance. The direct-on-line configurations were done on the Maxwell-2D model. The number of rotor bars per pole is 6. Maxwell-2D takes a longer computational time to show the machine performances, the machine was allowed to run for 6 seconds with the application of 30-Nm (70% the rated load) load at 3-second.

In the FEM calculations, the rotating members (rotor, shaft and rotor bars) were shifted to distort the air gap distribution to create an eccentricity fault in the direction shown in Fig. 9. All the rotating parts were moved from the origin at some distances of 0.04 mm, 0.16 mm and 0.32 mm representing 10%, 40% and 80% of the air gap length of 0.4 mm in the same direction. A new coordinate system was created with its centre in the centre of the now displaced rotating member. The motion setup was changed to rotate around the new coordinate system involving eccentricity.

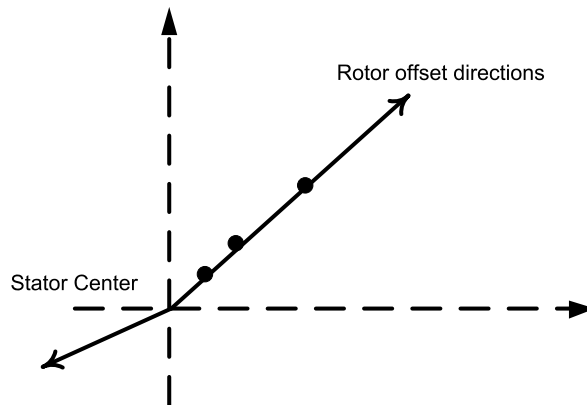
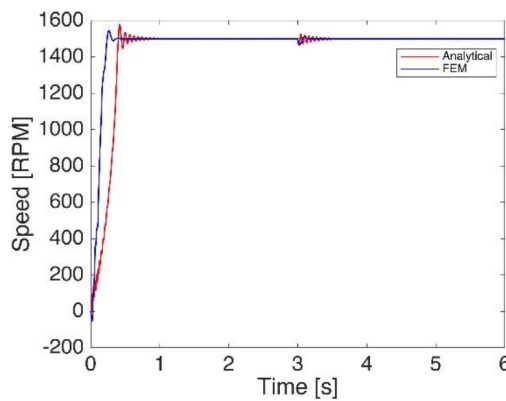


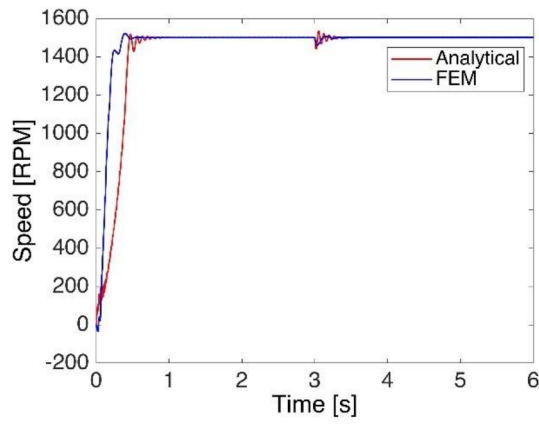
Fig. 9. Position of stator and rotor origin

5. Dynamic simulation results

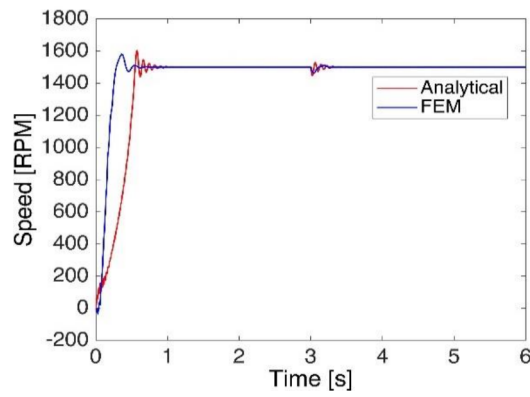
The phase variable method and FEM results showing the machine performances are presented side by side for clarity and comparison. A unit step load of 30 Nm was applied to the motor in both cases as shown in Figs. 10 to 12. The results are for healthy and unhealthy (eccentric) SynRM as indicated in the figures. The values of the inverse air gap and the inductance plots were used in the developed algorithms for the two conditions in the phase variable model. The algorithms were arbitrarily developed for the healthy, 10% and 40%. Attempt to increase the eccentricity to 80% stalled the rotor and further plots on the case could not be presented. The results are grouped for brevity to show the performance of the machine in terms of the speed, electromagnetic torque, torque-speed, and phase-A stator current characteristics and are validated using FEM.



(a) Healthy machine

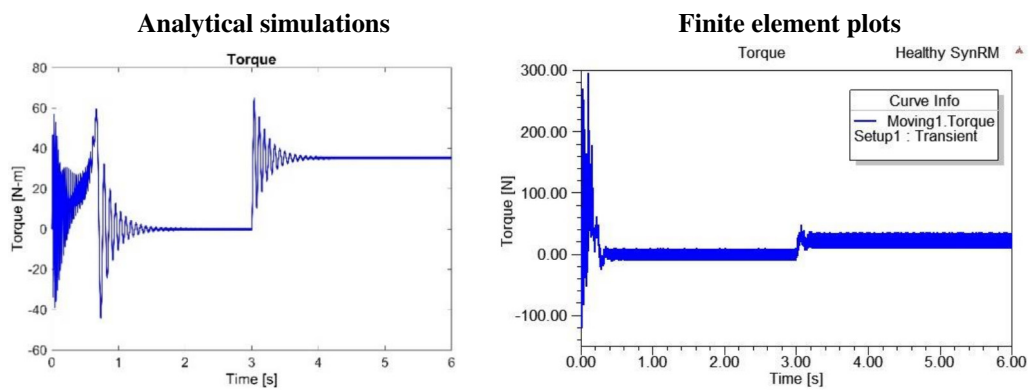


(b) 10% eccentricity

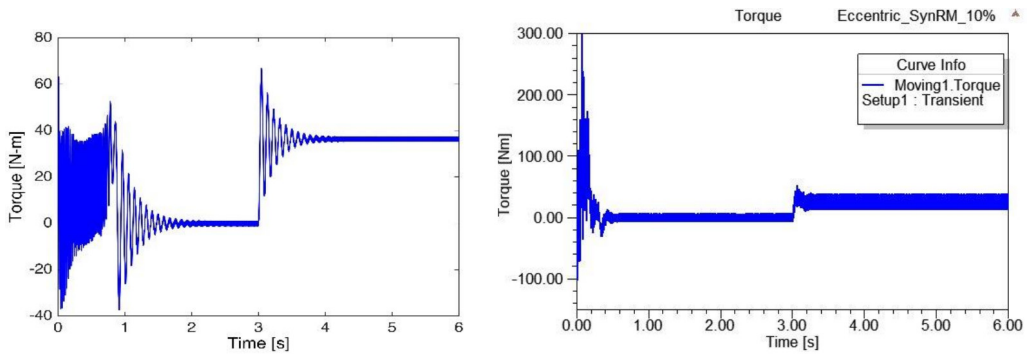


(c) 40% eccentricity

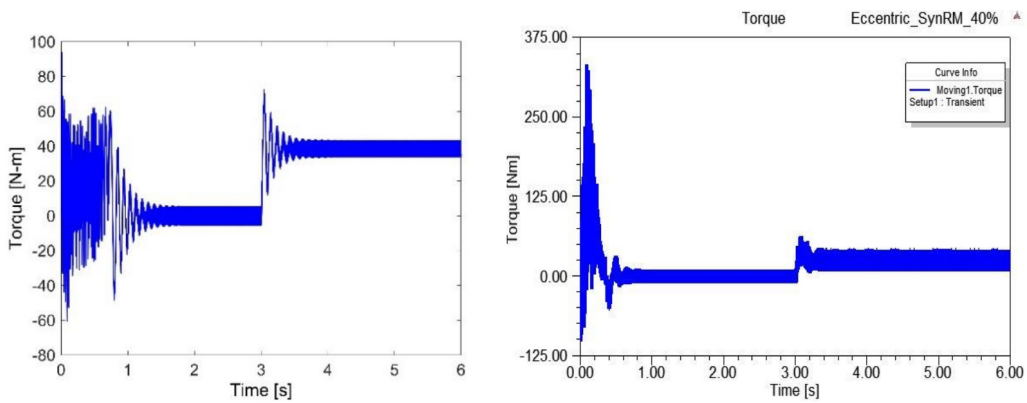
Fig. 10. Speed of SynRM



(a) Healthy machine

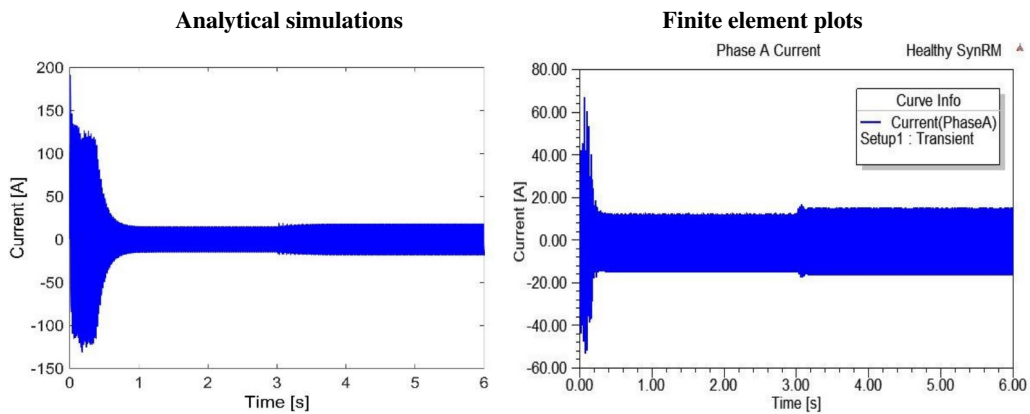


(b) 10% eccentricity



(c) 40% eccentricity

Fig. 11. Torque of SynRM (left: analytical method; right: validation using FEM)



(a) Healthy machine

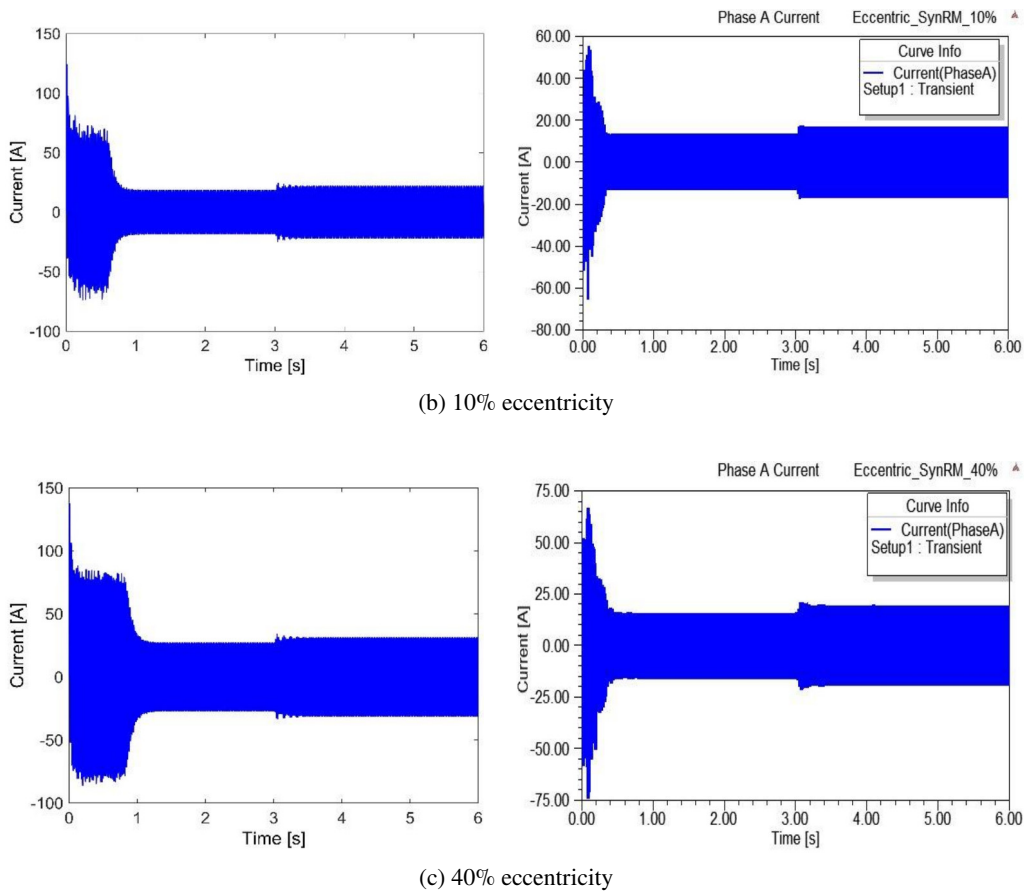


Fig. 12. Stator current of SynRM (left: analytical method; right: validation using FEM)

6. Discussion of results

The simulations were done with a constant voltage supply of 370 V, 50 Hz in MATLAB/SIMULINK environment and ANSYS Maxwell-2D at a fixed load torque of 30 Nm. The results of the analytical method were achieved by inputting the values of the inverse air-gap function generated in Fig. 3 and the values of the inductances into the developed phase-variable method algorithms. Also, the finite element method results were gotten by configuring the SynRM in ANSYS by employing the machine dimensions and parameters on RMxprt before converting it to 2D-Maxwell. The 2D-Maxwell was allowed to run which generated the results required for validation. Because ANSYS takes a longer computational time to show the machine performance, the load torque was introduced at $t = 3.0$ seconds for the phase variable model. The results of the machine performance were grouped for brevity to show the comparison of the performance index at chosen values of static eccentricity faults. The results show that the time duration for the

machine to perform its task is lesser for the healthy machine which is expected. Operating the ANSYS Maxwell 2D at 80% eccentricity fault showed an intersection of parts which implied the machine severity point.

The degree of eccentricity clearly manifests in all the inductances (self and mutual) plots of Figs. 4–8. However, this parameter even though it varies clearly with rotor position and highly indicative, does not present itself as a measurable quantity in the machine terminals under dynamic modes.

The speed versus time plot is shown in Fig. 10. The results show that the machine became stable after attaining synchronous speed at different times. It took the healthy SynRM 1.189 secs, while the SynRM operating at 10% and 40% took 1.389 s and 1.724 s respectively on no-load conditions but the SynRM operating at 80% eccentricity fault, was characterized by severe acoustic noise and vibrations for a longer time without attaining synchronous speed on no-load condition. The applied step load is the reason for the synchronous speed disappearance which was damped by the rotor cage after a little while but lost stability in the case of the 80% eccentric SynRM due to its severity. The FEM results confirm the results as the values closely matched that of the phase variable model.

The torque as an important index to judge SynRM performance is presented in Fig. 11. This shows results for the healthy, 10% and 40% eccentricity fault machines. It is evident from the plots that, the starting torque of the 10% eccentric SynRM compared with the healthy motor increased by 12.22 Nm which represents an increase of 23.4% and 58.8% for the 40% eccentric machine. Excess vibrations and noise were recorded for the case of the 80% eccentric SynRM. At a steady state no-load conditions, there is an insignificant value of increase on the torque as the fault increases. At the application of the load, the analytical and FEM results showed a momentary increase of torque as indicated in Fig. 11 while at 80% fault, the ripples surmounted the machine and made it unstable.

Finally, the study of the effect of the fault on stator current is shown in Fig. 12. On no-load condition, the current profile of the healthy SynRM was stable for the phase variable and FEM respectively. It is obvious, that at no-load condition, the steady state current is not significantly affected but generates a current profile that existed longer than the healthy machine as shown by both FEM and analytical methods. On-load condition, again the results showed that the average currents increased at steady states.

7. Conclusion

The analysis and simulated results show the influence of static eccentricity fault on the performance of the synchronous reluctance motor. The effect of eccentricity was most clearly manifested in the inductances calculated. The performance characteristics for the phase variable model and the FEM are closely matched. The FEM results are; however, more accurate than the analytical model. The results demonstrated that static eccentricity has a significant impact on the machine performance, especially when allowed to escalate. This is revealed by the increased starting torque and ripples generated by the faulty machine that caused it to execute a given task at a longer time. Apart from that, it was shown that the windings of the machine are exposed to danger as higher current harmonics are generated and recorded in the faulty machine. It was

also established that, as the fault increased, the performance indicators of the machine were also affected. The severity of the fault manifested as the fault approached 80% making the machine lose its stability. Therefore, to avoid rubbing the stator and rotor as the fault increases, the fault should be corrected at the early stage to elude downtime.

References

- [1] Kiani M., Lee W-J., Kenarangui R., Fahimi B., *Detection of Rotor Faults in Synchronous Generators*, 2007 IEEE International Symposium on Diagnostics for Electric Machines, pp. 266–271 (2007), DOI: [10.1109/DEMPED.2007.4393106](https://doi.org/10.1109/DEMPED.2007.4393106).
- [2] Ebrahimi B.M., Faiz J., *Configuration Impacts on Eccentricity Fault Detection in Permanent Magnet Synchronous Motors*, IEEE Transactions on Magnetics, vol. 48, no. 2, pp. 903–906 (2012), DOI: [10.1109/TMAG.2011.2172977](https://doi.org/10.1109/TMAG.2011.2172977).
- [3] Obe E.S., Binder A., *Direct-phase-variable model of a synchronous reluctance motor including all slot and winding harmonics*, Energy Conversion and Management, vol. 52, no. 1, pp. 284–291 (2011), DOI: [10.1016/j.enconman.2010.06.069](https://doi.org/10.1016/j.enconman.2010.06.069).
- [4] Obe E.S., Onwuka I.K., *Modelling and performance of a self-excited two-phase reluctance generator*, Nigerian Journal of Technology, vol. 30, no. 2, pp. 55–66 (2011).
- [5] Hamiti T., Lubin T., Baghli L., Rezzoug A., *Modeling of a synchronous reluctance machine accounting for space harmonics in view of torque ripple minimization*, Mathematics and Computers in Simulation, vol. 81, no. 2, pp. 354–366 (2010), DOI: [10.1016/j.matcom.2010.07.024](https://doi.org/10.1016/j.matcom.2010.07.024).
- [6] Lin I.H., Hsieh M.F., Kuo H.F., Tsai M.C., *Improved Accuracy for Performance Evaluation of Synchronous Reluctance Motor*, IEEE Transactions on Magnetics, vol. 51, no. 11, pp. 1–4 (2015), DOI: [10.1109/TMAG.2015.2450255](https://doi.org/10.1109/TMAG.2015.2450255).
- [7] Ojaghi M., Nasiri S., *Modeling Eccentric Squirrel-Cage Induction Motors with Slotting Effect and Saturable Teeth Reluctances*, IEEE Transactions on Energy Conversion, vol. 29, no. 3, pp. 619–627 (2014), DOI: [10.1109/TEC.2014.2320823](https://doi.org/10.1109/TEC.2014.2320823).
- [8] Polat A., Yilmaz A., Ergene L.T., *Investigation of The Effects of Eccentricity on Induction Motor via Multi-Resolution Wavelet Analysis*, Electrica, vol. 18, pp. 187–197 (2014), DOI: [10.5152/iu-jeee.2018.1821](https://doi.org/10.5152/iu-jeee.2018.1821).
- [9] Silwal B., Rasilo P., Belahcen A., Arkkio A., *Influence of the rotor eccentricity on the torque of a cage induction machine*, Archives of Electrical Engineering, vol. 66, no. 2, pp. 383–396 (2017), DOI: [10.1515/ae-2017-0029](https://doi.org/10.1515/ae-2017-0029).
- [10] Karami M., Mariun N., Mehrjou M.R., Ab-Kadir M.Z.A., Mison N., Amran M., Radzi M., *Static Eccentricity Fault Recognition in Three-Phase Line Start Permanent Magnet Synchronous Motor Using Finite Element Method*, Mathematical Problems in Engineering, vol. 2014, article ID 132647 (2014), DOI: [10.1155/2014/132647](https://doi.org/10.1155/2014/132647).
- [11] Jaeger M., Drichel P., Schröder M., Berroth J., Jacobs G., Hameyer K., *On magnetization deviations as the dominant cause for vibration harmonics in the spectrum of a PMSM drive*, Archives of Electrical Engineering, vol. 70, no. 3, pp. 719–730 (2021), DOI: [10.24425/ae.2021.137584](https://doi.org/10.24425/ae.2021.137584).
- [12] Huang Y., Guo B., Hemeida A., Sergeant P., *Analytical Modeling of Static Eccentricities in Axial Flux Permanent-Magnet Machines with Concentrated Windings*, Energies, vol. 9, no. 892, pp. 1–19 (2016), DOI: [10.3390/en9110892](https://doi.org/10.3390/en9110892).
- [13] Xiong G., Hou Y., Fang P., Du M., *Stability and Synchronous Characteristics of Dual-Rotors Vibrating System Considering the Material Effects*, Journal of Vibration Engineering and Technologies, vol. 10, pp. 1665–1678 (2022), DOI: [10.1007/s42417-022-00472-5](https://doi.org/10.1007/s42417-022-00472-5).

- [14] Taghipour Boroujeni S., Jalali P., Bianchi N., *Analytical Modeling of No-Load Eccentric Slotted Surface-Mounted PM Machines: Cogging Torque and Radial Force*, IEEE Transactions on Magnetics, vol. 53, no. 12, pp. 1–8 (2017), DOI: [10.1109/TMAG.2017.2748501](https://doi.org/10.1109/TMAG.2017.2748501).
- [15] Hooshmandi H., Ebrahimi J.K., Davoudi A., Pouramin A., *Analytical Derivation of Induction Motors Inductances under Eccentricity Conditions*, Progress in Electromagnetics Research, vol. 60, pp. 95–110 (2014), DOI: [10.2528/PIERB14051704](https://doi.org/10.2528/PIERB14051704).
- [16] Obe E.S., *Direct computation of ac machine inductances based on winding function theory*, Energy Conversion and Management, vol. 50, no. 3, pp. 539–542 (2009), DOI: [10.1016/j.enconman.2008.10.017](https://doi.org/10.1016/j.enconman.2008.10.017).
- [17] Akbari H., Milimonfared J., *An evaluation of inductances of a salient pole synchronous machine under different axial eccentricity conditions*, European Transactions on Electric Power, vol. 23, no. 4, pp. 1–16 (2012), DOI: [10.1002/etep.1613](https://doi.org/10.1002/etep.1613).
- [18] Hamdani S., Touhami O., Ibtouen R., Hasni M., *Analytical evaluation of inductances for induction machine with dynamic eccentricity using MWFA and FE methods*, Proc. – 2013, 9th IEEE International Symposium on Diagnostics Electric Machines, Power Electronics and Drives, SDEMPED 2013, pp. 420–427 (2013), DOI: [10.1109/DEMPED.2013.6645750](https://doi.org/10.1109/DEMPED.2013.6645750).
- [19] Serrano-Iribarnegaray L., Cruz-Romero P., Gomez-Exposito A., *Critical Review of the Modified Winding Function Theory*, Progress In Electromagnetics Research, vol. 133, pp. 515–534 (2013), DOI: [10.2528/PIER12091301](https://doi.org/10.2528/PIER12091301).
- [20] Toliyat H.A., Al-Nuaim N.A., *Simulation and Detection of Dynamic Synchronous Machines*, IEEE Transactions on Industry Applications, vol. 35, no. 1, pp. 86–93 (1999), DOI: [10.1109/28.740849](https://doi.org/10.1109/28.740849).
- [21] Akbari H., *An improved analytical model for salient pole synchronous machines under general eccentricity fault*, Progress In Electromagnetics Research, vol. 49, pp. 389–409 (2013), DOI: [10.2528/PIERB13010101](https://doi.org/10.2528/PIERB13010101).
- [22] Akbari H., *Analytical computation of reluctance synchronous machine inductances under different eccentricity faults*, Progress in Electromagnetics Research, vol. 24, pp. 29–44 (2012), DOI: [10.2528/PIERM11102005](https://doi.org/10.2528/PIERM11102005).
- [23] Hwang C.M.C., Chenga S.P., Chana C.K., Pan C.T., Chang T.Y., *Comparison of performances between IPM and SPM motors with rotor eccentricity*, Journal of Magnetism and Magnetic Materials, vol. 282, pp. 360–363 (2004), DOI: [10.1016/j.jmmm.2004.04.084](https://doi.org/10.1016/j.jmmm.2004.04.084).
- [24] Wu X., Zhu Z.Q., Wu Z.Y., Liu T.Y., Li Y.X., *Analysis and Suppression of Rotor Eccentricity Effects on Fundamental Model Based Sensorless Control of Permanent Magnet Synchronous Machine*, IEEE Transactions on Industry Applications Analysis, vol. 9994, pp. 1–10 (2020), DOI: [10.1109/TIA.2020.2997297](https://doi.org/10.1109/TIA.2020.2997297).
- [25] Takahata R., Wakui S., *Influence of Rotor Eccentricity on Vibration Characteristics of Permanent Magnet Synchronous Motor*, IEEE Journal of Industry Applications, vol. 8, no. 3, pp. 558–565 (2019), DOI: [10.1541/ieejia.8.558](https://doi.org/10.1541/ieejia.8.558).
- [26] Iamamura B.A.T., Le-Menach Y., Tounzi A., Sadowski N., Guillot E., *Study of static and dynamic eccentricities of a synchronous generator using 3-D FEM*, IEEE Trans. Magnetics, vol. 45, no. 8, pp. 3516–3519 (2010), DOI: [10.1109/TMAG.2010.2043347](https://doi.org/10.1109/TMAG.2010.2043347).
- [27] Faiz J., Pakdelian S., *Finite Element Analysis of Switched Reluctance Motor under Dynamic Eccentricity Fault*, IEEE Transactions on Magnetics, vol. 42, no. 8, pp. 2004–2008 (2006), DOI: [10.1109/TMAG.2006.875997](https://doi.org/10.1109/TMAG.2006.875997).
- [28] Al-Nuaim N.A., Toliyat H.A., *A Method for Dynamic Simulation and Detection of Dynamic Air-Gap Eccentricity in Synchronous Machines*, 1997 IEEE International Electric Machines and Drives Conference Record, pp. MA2/5.1-MA2/5.3 (1997), DOI: [10.1109/IEMDC.1997.604067](https://doi.org/10.1109/IEMDC.1997.604067).

- [29] Tootoonchian F., Abbaszadeh K., Ardebili M., *A New Technique for Analysis of Static Eccentricity*, Journal of Measurement Science Review, vol. 12, no. 1, pp. 14–20 (2012), DOI: [10.2478/v10048-012-0004-y](https://doi.org/10.2478/v10048-012-0004-y).
- [30] Bessous N., Zouzou S.E., Sbaa S., *Static Eccentricity Fault Detection of Induction Motors using MVSA, MCSA and Discrete Wavelet Transform (DWT)*, The 5th International Conference on Electrical Engineering – Boumerdes (ICEE-B), Boumerdes, Algeria, October 29–31 (2017), DOI: [10.1109/ICEE-B.2017.8192035](https://doi.org/10.1109/ICEE-B.2017.8192035).
- [31] Wroński W., Sułowicz M., Dziechciarz A., *Dynamic And Static Eccentricity Detection In Induction Motors In Transient States*, Technical Transactions Electrical Engineering, pp. 171–193 (2015), DOI: [10.4467/2353737XCT.15.095.3927](https://doi.org/10.4467/2353737XCT.15.095.3927).
- [32] Aggarwal A., Strangas E.G., *Review of Detection Methods of Static Eccentricity for Interior Permanent Magnet Synchronous Machine*, Energies, vol. 12, no. 4105, pp. 1–20 (2019), DOI: [10.3390/en12214105](https://doi.org/10.3390/en12214105).
- [33] Dogan Z., Emeksiz C., Burak K., Gokrem L., *The Static Eccentricity Fault Diagnosis in Time Domain at Line Start Permanent Magnet Synchronous Motor*, Journal of New Results in Science, vol. 12, pp. 88–95 (2016).
- [34] El M., Oumaamar K., Maouche Y., Boucherma M., *Static air-gap eccentricity fault diagnosis using rotor slot harmonics in line neutral voltage of three-phase squirrel cage induction motor*, Mechanical System Signal Process, vol. 84, pp. 584–597 (2017), DOI: [10.1016/j.ymsp.2016.07.016](https://doi.org/10.1016/j.ymsp.2016.07.016).
- [35] Toliyat H.A., Arefeen M.S., Parlos A.G., *A method for dynamic simulation of air-gap eccentricity in induction machines*, IEEE Transactions on Industry Applications, vol. 32, no. 4, pp. 910–918 (1996), DOI: [10.1109/28.511649](https://doi.org/10.1109/28.511649).
- [36] Lipo T.A., *Analysis of Synchronous Machines*, New York: CRC Press (2017).
- [37] Bouabid N., Moussa M.-A., Maouche Y., Khezzar A., *The effect of closed loop control on diagnostic indices in different faults of squirrel cage induction motor*, Archives of Electrical Engineering, vol. 70, no. 4, pp. 943–958 (2021), DOI: [10.24425/ae.2021.138271](https://doi.org/10.24425/ae.2021.138271).
- [38] Faiz J., Ebrahimi B.M., Valavi M., *Mixed Eccentricity Fault Diagnosis In Salient-Pole Synchronous Generator Using Modified Winding Function Method*, Progress In Electromagnetics Research B, vol. 11, pp. 155–172 (2009), DOI: [10.2528/PIERB08110903](https://doi.org/10.2528/PIERB08110903).